Deep-Sea Research II 119 (2015) 61–68

Contents lists available at ScienceDirect

Deep-Sea Research II

journal homepage: www.elsevier.com/locate/dsr2

On the variability of tidal fronts on a macrotidal continental shelf, Northern Patagonia, Argentina

Juan P. Pisoni [a,*], Andrés L. Rivas [a,b], Alberto R. Piola [c,d]

[a] Centro Nacional Patagónico (CENPAT-CONICET), Argentina
[b] Fac. Cs. Naturales (UNPSJB), Argentina
[c] Servicio de Hidrografía Naval, Universidad de Buenos Aires, Argentina
[d] Instituto Franco-Argentino sobre Estudios del Clima y sus Impactos (CONICET), Argentina

ARTICLE INFO

Available online 6 February 2014

Keywords:
Tidal front
Tidal mixing
Surface temperature
Spring–neap cycle
Shelf sea
Biological–physical interactions
Remote sensing
Patagonian shelf
Patagonia Argentina

ABSTRACT

Tidal fronts are associated with the transition between homogeneous and vertically stratified water and are characterized by the simultaneous availability of light and nutrients that enhance the growth of marine productivity. We study the variability in the position of two tidal fronts located in Patagonia Argentina: the San Matías and Valdés fronts. The rate of tidal dissipation in these regions is among the highest of the world oceans. The study is based on the analysis of over 1200 satellite derived sea surface temperature images. The results indicate that the mean monthly position of both fronts is strongly linked to the characteristics of the bottom topography. In response to increasing surface heat flux the fronts displace toward shallower areas. Similarly, a slight displacement towards deeper waters is observed when the heat flux decreases. High frequency variability is revealed by the standard deviation around monthly averages. At the mouth of the San Matías gulf, the front location variability in the spring–neap cycle is around 10 km, while east of the Valdés Peninsula the fortnightly cycle is masked by high frequency fluctuations (~30 km) governed by meanders and meso-scale filaments. A simple conceptual model is proposed which suggests that the mean frontal position is determined by the bottom topography while its seasonal variability is driven by the surface heat flux, and the front intensity is modulated by the spring–neap transition.

1. Introduction

During the last 30 years, satellite images have been used to observe patterns in frontal areas that were difficult to observe from in-situ data. Since the early spacecraft missions returned images of the surface ocean revealing convoluted patterns, thermal fronts have been recognized as ubiquitous features of the sea surface (Apel, 1980).

However, few studies have addressed the high-frequency variability (~1 month) of thermal fronts. The early work of Pingree (1978) described the formation of cyclonic eddies in the Ushant frontal system in the Celtic Sea. Later, Pingree (1979) reported that tidal fronts occasionally displayed cold filaments as a result of local instabilities. Recently, Hopkins and Polton (2012) observed fortnightly and semidiurnal superimposed variability in the position of a thermohaline front off Liverpool Bay, associated with tidal mixing variations.

Simpson and Bowers (1981) emphasized the analogy between tidal fronts observed around the United Kingdom shelf and those in other regions of high tidal dissipation. They discussed the extrapolation of their results to other regions. Notwithstanding the dynamic similarities between tidal fronts, the quantification in space and time of local fluctuations is essential to understand their contribution to local productivity.

The northern area of the Argentine Continental Shelf (ACS) is characterized by an annual net positive heat flux, strong seasonal vertical stratification (Rivas, 1990), strong winds (Hoffman et al., 1997), and high tidal energy dissipation (Egbert et al., 2004). Glorioso and Simpson (1994) estimated that the M_2 tidal dissipation from the northern sector of the Atlantic Patagonia contributes to about 5.3% of the global energy dissipation, which is comparable to the contribution from the North Sea (Davis et al., 1985). Tidal dissipation throughout the shelf derived from a numerical simulation by Glorioso and Flather (1997) is around 230 GW. A more recent model employing near bottom velocities and an embedded turbulent closure scheme to parameterize vertical

* Correspondence to: Centro Nacional Patagónico (Consejo Nacional de Investigaciones Científicas y Técnicas de Argentina), Bvd. Brown 2915, U9120ACF Puerto Madryn, Argentina. Tel: +54 280 451024.
E-mail address: pisoni@cenpat.edu.ar (J.P. Pisoni).

http://dx.doi.org/10.1016/j.dsr2.2014.01.019
0967-0645

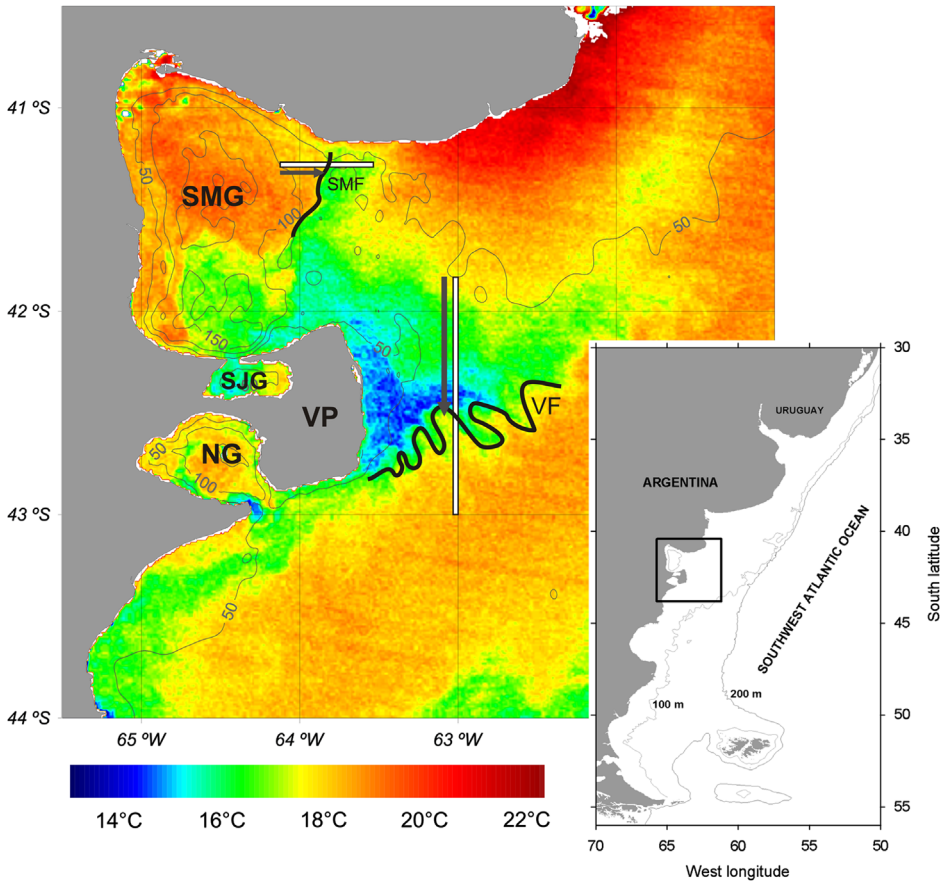

Fig. 1. NOAA-AVHRR sea surface temperature (SST) image of the North Patagonian area on 16 January 2002. Heavy black lines show the schematic representation of the SMF and the VF based on the approximate location of the region where SST gradient is $> 0.14\ ^{\circ}C\ km^{-1}$. The straight white lines indicate the positions of the SST transects. Arrows represent the distance to the fronts. Contours indicate the bathymetry (in meters). **VP**: Valdés Peninsula; **SMG**: San Matías Gulf; **SJG**: San José Gulf and **NG**: Nuevo Gulf.

mixing leads to smaller dissipations (110 GW, Palma et al., 2004). Regardless of the discrepancies of the mean dissipation rates, all the above simulations present very inhomogeneous distributions of dissipation of the M_2 tidal component, and locate the largest rates in northern Patagonia along a narrow strip extending northeastward from the Valdés Peninsula (VP, Fig. 1) (e.g. Glorioso and Simpson, 1994; Glorioso and Flather, 1997; Palma et al., 2004).

As suggested by Polzin et al. (1997) a pattern of enhanced vertical mixing associated with the interaction of tidal currents and rough bathymetry is expected. In agreement with these direct observational results the studies of Egbert and Ray (2000, 2001) indicate enhanced tidal dissipation over large-scale topographic features. The San Matías Gulf (SMG) located north of VP has a maximum depth of around 200 m, while the sill depth near the mouth is ~70 m. Based on surface roughness observations derived from remote sensing, Gagliardini et al. (2005) described rough bed forms in the topography near the SMG mouth and VP. They also report that echosounder surveys carried out by Argentina's Servicio de Hidrografía Naval in 1959 revealed sand waves of 10 m height and 600 m wavelength at nearly 80 m depth at these locations. Similarly, Pierce et al. (1969) found a series of large sand waves as high as 17 m and 680 m wavelength at the entrance of the SMG at a depth lower than 90 m. Since bottom topographic features of these scales cannot be resolved by the above-mentioned numerical simulations, real tidal mixing may exceed the available estimates derived from the models.

In late Austral spring and summer the region of high tidal dissipation is bounded by relatively intense thermal fronts (Rivas and Pisoni, 2010). These fronts develop at the interface among relatively shallow, well-mixed and stratified waters. Along its southern edge is the Valdés front (VF, Fig. 1). The VF extends northeastward from the southern VP (Carreto et al., 1986; Acha et al., 2004; Sabatini and Martos, 2002, among others) and matches the boundary between the Argentinean and the Magellan biogeographical provinces (Balech and Ehrlich, 2008). The high chlorophyll-a concentration (Acha et al., 2004; Romero et al., 2006; Rivas et al., 2006) and the large number of fish species observed around the VF suggest that this region is among the richest in the ACS (Alemany et al., 2009). The impact of the VF on the phytoplankton abundance manifests itself in the sea–air CO_2 fluxes, which switch from emission to the atmosphere in the onshore (well mixed) side to uptake on the offshore side (Bianchi et al., 2009). The western edge of the high tidal dissipation region is marked by a front located along the north of the SMG mouth (SMF, Fig. 1). The SMF is characterized by high chlorophyll-a concentrations (Williams et al., 2010) and concentrates significant fishing efforts (Ocampo-Reinaldo et al., 2013).

The location of thermal fronts in the ACS has been determined in a number of studies based on the analysis of relatively low spatial ($>$ 4 km) and temporal (weekly–monthly) resolutions (Bava et al., 2002; Acha et al., 2004; Rivas, 2006; Rivas and Pisoni, 2010; among others). The large tidal dissipation approaching the coast leads to intense vertical mixing (Glorioso and Flather 1995; Palma et al., 2004) and the seasonal formation of relatively intense tidal fronts (Rivas and Pisoni, 2010). The alternation between homogeneous and vertically stratified water, usually associated with tidal fronts, impacts the availability of light and nutrients, thus enhancing marine primary productivity. Consequently, these regions are also usually associated with significant fishing grounds (Podestá et al., 1993; Bogazzi et al., 2005). Given

Table 1
Number of images per year used in this study.

Year	1999	2000	2001	2002	2003	2004	2005	2006	2007	2008
Number of images	31	109	171	136	104	93	128	155	167	118

Table 2
Threshold gradients for both transects.

Transect	TGr (°C km^{-1})
SMF	0.142
VF	0.116

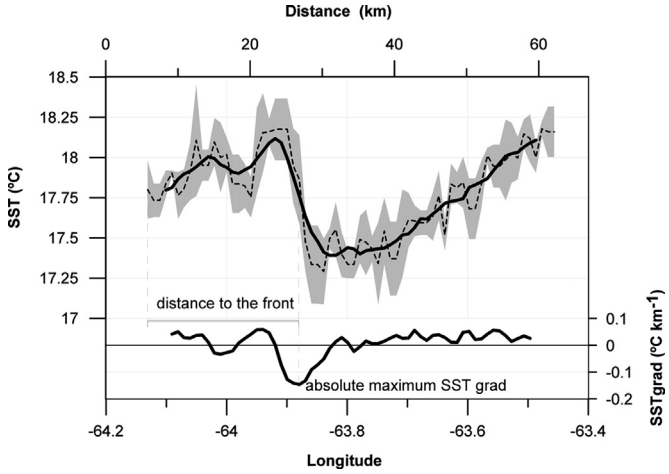

Fig. 2. Sea surface temperature across the SMF on 16 February 2000. The average temperature calculated over five transverse pixels (dotted line), its standard deviation (gray shading) and a 7 element running average (heavy line) are shown. The lower panel (right axis) is the cross-front temperature gradient used to determine the front position and intensity.

the significant role of tidal fronts on the shelf ecology and circulation it is important to quantify and understand what processes cause the frontal variability. In this paper we analyze the variability of two tidal fronts located in the region of the largest tidal dissipation in the northern Patagonian shelf (Fig. 1) and explore the possible causes of the observed variability. Using all the available daily AVHRR images we analyzed the spatio-temporal changes experienced by both fronts with the best possible resolution.

2. Data and methods

The study is based on the analysis of daily satellite images of sea surface temperature (SST) of 1.1 km of spatial resolution collected during the period 1999–2008. These AVHRR images, obtained from NOAA satellites 12, 14, 15, 16, 17 and 18 (Table 1), were provided by the Comisión Nacional de Actividades Espaciales (CONAE, Argentina) and processed at the Centro Nacional Patagónico (CENPAT, Argentina). All AVHRR images were corrected for geometric distortion (RMSE $\leq$ 0.55 pixel), mapped to a WGS84 reference system (datum WGS84, ellipsoid WGS84) and co-registered with a reference landmask. Clouds were removed using a combination of threshold values from channels 2 and 4 (Kelly, 1985; Monaldo, 1996) and flagged to zero. For further reference on processing of satellite data see Williams et al. (2010). Individual images rather than composites were analyzed in order to optimize the space-time resolution required to resolve high frequency frontal displacements.

To explore the frontal displacements in response to the combined effect of tidal mixing and surface momentum and heat fluxes we use a simple one-dimensional turbulence-closure numerical model adapted from Sharples (1999). The model solves numerically the simplified momentum conservation equations including a term of oscillating sea surface slope that drives the tidal currents, the Coriolis and mixing terms. To provide a link between vertical stability (driven by seasonal solar heating) and vertical mixing (driven by tidal currents and surface wind stress) the model employs a level 2.2b turbulence closure scheme from Simpson et al. (1996). The scheme provides a non-arbitrary method to relate the local stability of the water column to the efficiency of the vertical turbulent transport. The model was forced using the wind and surface heat fluxes from National Centers for Environmental Prediction reanalysis (NCEP, Kalnay et al., 1996). The tidal forcing varies node to node in the model but the atmospheric forcings were assumed to be representative of the region ($\sim$100 km). Details of the model configuration are given in Section 4 and Sharples and Tett (1994).

To analyze the relative position of the fronts and their temporal fluctuations, we selected two cross-front transects (Fig. 1). These transects were selected based on the analysis of more than 1200 satellite SST images collected during a 10 year period (Table 1). The transects span regions where fronts are more frequently detected and may not necessarily coincide with the area of the greatest frontal displacement. A zonal transect crosses the SMF at the SMG mouth, centered at 41.35°S between 64.14°W and 63.45°W. The other transect crosses the VF meridionally at 63.05°W between 41.8°S and 43°S (Fig. 1). To reduce the image noise SST transects were constructed averaging 5 pixels in the cross-transect direction. Thus, each SST transect represents a strip $\sim$5.5 km wide. In addition, to minimize the error in the frontal position due to noise in the data, temperatures along each transect were smoothed using a 7 element centered moving average. This averaging scale was determined by trial and error as the smallest amount of elements for unequivocal detection of the fronts. The frontal position in each SST image was determined as the distance from the first transect point (indicated by arrows in Fig. 1) to the point of maximum cross-front (along-transect) SST gradient (Fig. 2). The SST gradient was estimated by finite differences as

$$\nabla SST_k = \frac{SST_{k+1} - SST_{k-1}}{\Delta dist_k} \quad (1)$$

where ∇SST represents the SST gradient and $\Delta dist_k$ represents the cross-frontal distance between pixels $k+1$ and $k-1$. The distance was calculated only if the maximum absolute variation of SST exceeded a certain threshold. The threshold was set as the average of the maximum absolute values of the gradients on each transect during the record length (Table 2). Only images that were completely cloud free on each transect were used. Since cloudiness increases in winter the number of images used exhibits some seasonality. To reduce this seasonal effect the frontal frequency was calculated as the percent of frontal images (SST gradient greater than the threshold) relative to the number of images available in that month.

3. Results

3.1. Frontal location and monthly variability

The tidal SMF is located on the mouth of SMG (Fig. 1). The balance between buoyancy fluxes by the incoming solar radiation,

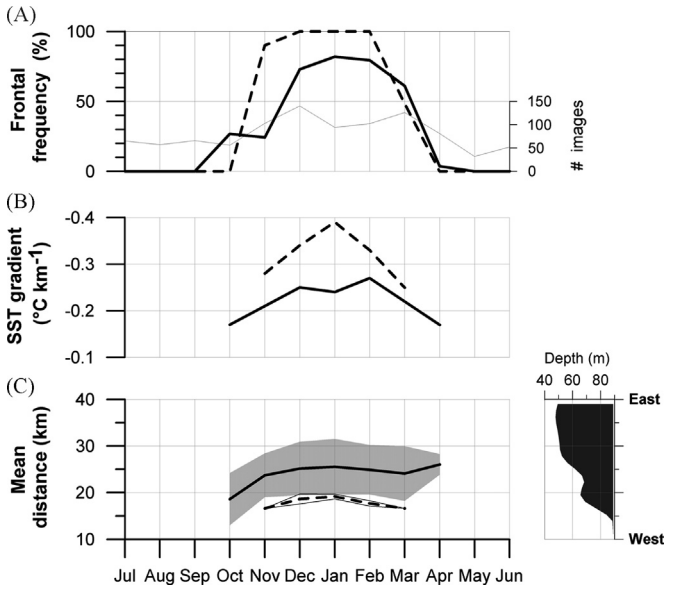

Fig. 3. Number of available images (thin line) and annual cycle of frontal frequency (A), mean gradient intensity (B) and mean monthly frontal position and their standard deviation (shaded area and thin lines) (C) at SMF. The solid lines show the estimates from SST images, dashed lines are estimates from the one-dimensional model. The inset shows the bathymetry along the transect.

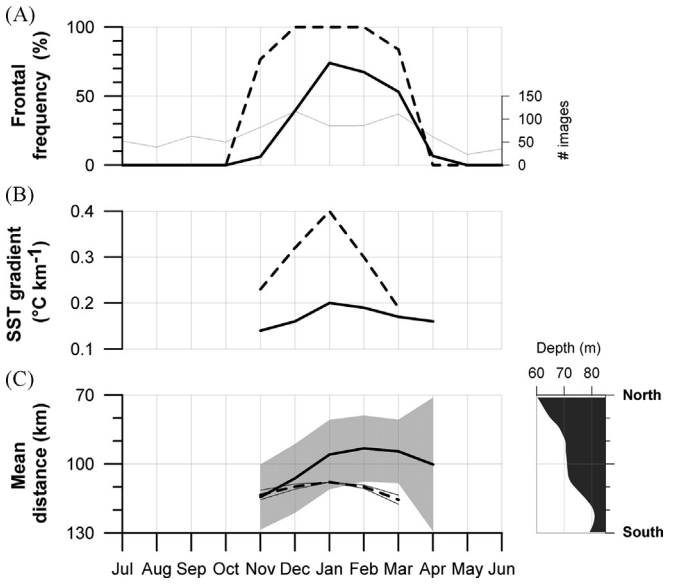

Fig. 4. As Fig. 3, for VF.

the turbulent tidal mixing and a marked change in depth are responsible for the generation of this tidal front (e.g. Glorioso and Simpson, 1994). The front is generated along the sill over the gulf mouth at the onset of vertical stratification associated with the increasing shortwave radiation. The southern part of the front is weakened by the inflow of relatively cold water from the shelf, which reduces the temperature contrast between the gulf and shelf waters (Gagliardini and Rivas, 2004; Tonini et al., 2013), and causes larger thermal gradients in the northern part of the mouth (Fig. 1). The front is evident in October, when it is observed in ~25% of the available images and reaches a high percentage of occurrence (> 60%) from December to March (Fig. 3A).

Over this transect the frontal detection is based on the analysis of 80% of the available images corresponding to the cloud-free images (Table 1). The maximum temperature gradient is observed in February, reaching an average of 0.27 °C km^{-1} (Fig. 3B). The frontal position is broadly constant from November to April, suggesting that the front is strongly influenced by the bathymetry. The displacement of the average monthly position of the front is smaller than the observed standard deviation (SD ~6 km, Fig. 3C). Nevertheless, this simple analysis suggests that the front displaces about 5 km eastward (e.g. to shallower waters) from October to January (Fig. 3C). The vertical stratification of temperature induced by the increasing surface heat flux during spring and early summer is the most probable explanation for the surface front displacement to shallower waters. Inversely, the slight westward displacement observed from February to March could be explained by the decreasing heat flux in late summer and early fall. During April the front is virtually undetectable (Fig. 3A), therefore its position is not considered in this analysis.

The transect that crosses the VF had 66% cloud-free images. The front is first detected in November, but is only observed in more than 50% of the images in January, February and March (Fig. 4A). This lower percentage of occurrence compared with the SMF could be explained by the relatively high gradient threshold estimated for this front. The front is located in its southernmost position in November. As the seasonal warming and vertical stratification increase, the front displaces approximately 20 km northward (to shallower waters). In March and April, the front moves slightly back to the south (Fig. 4C). The maximum temperature gradient is observed in January, reaching an average of 0.2 °C km^{-1} (Fig. 4b). As in the SMF, the displacement of the average monthly position of the front is lower than the observed standard deviation (SD~15 km, Fig. 4C), suggesting high levels of variability at higher frequencies.

3.2. Fortnightly variability

In fronts generated by turbulent tidal mixing, variability is expected to be partially associated with the spring–neap transition. Fortnightly displacement of fronts may contribute to an increased flow of nutrients across the front (Loder and Platt, 1985). In order to explore the association between the spring–neap tidal cycle and the front position, the anomaly of the front positions relative to the above-described monthly averaged positions was calculated for each image. Subsequently, these values were averaged for each day of the 29-day lunar cycle on which each image was taken. Averaged anomalies for each day of the lunar phase are shown in Fig. 5A and B for SMF and VF, respectively. To aid the visualization of the fortnightly cycle the daily averaged anomalies were smoothed with a 5-day running mean. We must point out that semidiurnal variations appear as noise in this analysis because the time at which the images were obtained was not taken into account. In addition to this fortnightly cycle, frontal movement occurs on semi-diurnal timescales; flood–ebb advection and tidal straining both alter the structure of the water column and the position of the front.

Hopkins and Polton (2012) find that the Liverpool Bay thermohaline front displaces 5–35 km in response to spring–neap changes in tidal mixing and undergoes semi-diurnal advective displacements of 5–10 km driven by flood and ebb tidal currents. The SMF oscillates approximately 10 km with fortnightly frequency (Fig. 5A). The maximum positive displacement (eastward, towards the shallower side of the front) occurs around full and new moons (Fig. 5A). Increased tidal currents imply greater vertical mixing, therefore, the front should move westward to deeper areas. Thus, these results suggest an age of the tide of about 7 days between spring tide (maximum current and mixing) and the full/new moon, or equivalently, a phase-lag of about 180° between the main semidiurnal lunar component (M_2) and the main semidiurnal solar component (S_2). The delay between the full and new moons and the following spring tide is called the age of the tide. A similar phase-lag (183°) has been observed by Tonini (2010)

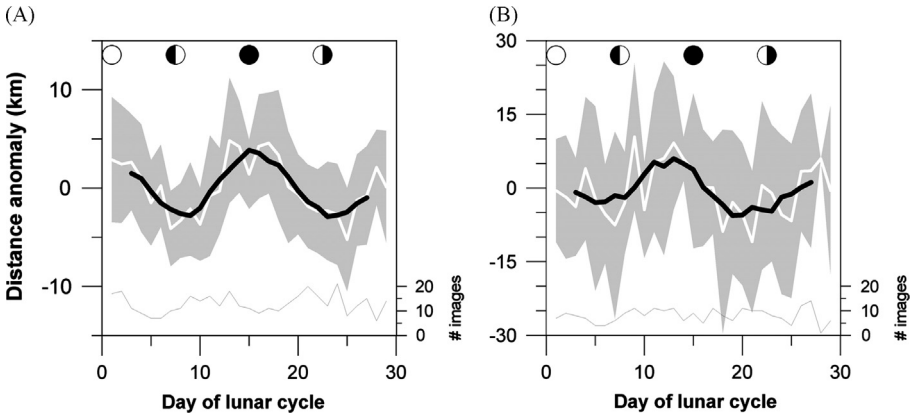

Fig. 5. Mean anomaly of the frontal location (relative to monthly means position, see text for details) for each day of the lunar cycle (white line) and 5-day running average (black line) for SMF (A) and VF (B). The shading indicates the standard deviations around the mean. Each panel shows the lunar phases at the top and the number of available images at the bottom (right axis).

based on a high-resolution numerical simulation. This observation implies that the phase-lag of the distances with respect to the full or new moon for the SMF transect is consistent with the modeled phase differences between the M_2 and S_2 components.

The fortnightly variation of the VF location is not well resolved due to the large standard deviation (Fig. 5B). However, there are differences of up to 20 km between the new moon and first quarter, although the SD is also quite large (~13 km). The maximum distances (positive anomalies) were recorded around the new and full moon (Fig. 5B) and this situation should be expected during spring tides, when a stronger vertical mixing would lead to a southward front displacement (to deeper waters). Hence, these results suggest that semidiurnal M_2 and S_2 components are in phase, and spring tides are approximately coincident with the new and full moon. According to the model implemented by Tonini (2010), the average phase-lag between semidiurnal components M_2 and S_2 is about 5° which corresponds to an age of the tide of only ~5 h, which appears to be confirmed by our observation.

When interpreting the above-described results it should be noted that, given an increase in tidal current intensity, the magnitude of the frontal displacement also depends on the bottom slope (see Figs. 3 and 4). Our analysis suggests that average fortnightly oscillations of the fronts are higher than monthly oscillations, associated with the seasonal variation of the net surface heat flux and wind stress.

Additionally, the relatively high SD found even in fortnightly averaged frontal locations estimated from satellite data for the VF suggests significant variability at even higher frequencies. This variability could be influenced by the presence of filaments and meanders which are frequently observed in the SST images (see Fig. 1). Though these small-scale processes are observable in the SST images, their time variability cannot be properly resolved with the available data. Similar filaments have been observed in fronts in the Celtic Sea (Pingree, 1979), and may be associated with baroclinic instability processes along the front (Badin et al., 2009). Le Boyer et al. (2009) conclude that mixing effects bear a very strong influence on the thermal structure of the warm-water intrusions associated with frontal cyclonic eddies such as those described by Pingree (1979). Such fluctuations might enhance the local productivity. However, in-situ biological data with high spatial and temporal resolutions are essential to test this hypothesis.

4. Analysis of frontal variability based on a one-dimensional numerical model

A one-dimensional numerical model is used to analyze the role of the wind, tidal mixing and surface heat flux on the variability of the frontal positions. The model, developed by Sharples (1999), simulates the evolution of the vertical structure of the water column, based on the net surface heat flux and wind stress, and the tidal circulation. The model consists of a physical and a biological module. The physical module uses a second-order turbulence scheme as a link between the local vertical stability (generated by seasonal solar heating) and the vertical turbulent mixing (generated by tidal currents and surface winds). The model requires knowledge of the wind speed, the surface solar radiation and the dew point temperature to parameterize the heat exchange with a term proportional to the air–sea temperature difference. A detailed description of the model can be found in Sharples (1999). In this study, only the physical model was used, and the heat flux was estimated from shortwave, longwave, sensible and latent heat fluxes from the NCEP reanalysis (Kalnay et al., 1996). The effect of horizontal advection, liable to compensate the annual net heat gain by the sea (Rivas, 1994), is approximated by subtracting the average annual net heat flux in order to maintain the heat balance and a stationary annual mean temperature. The model is forced with daily values of wind and surface heat flux averaged from a 10-year climatology period. The use of smooth forcing eliminates a major source of variability but maintains the fundamental mechanisms and can be used to explore causal relationships. The bathymetry, the amplitude and the polarization (eccentricity and sense of rotation) of semidiurnal tidal components (M_2 and S_2) are obtained from nodes of a three-dimensional numerical model (Tonini, 2010), whose resolution is about 1.4 km.

The model was run for 30 nodes along the SMF transect, between 64°W and 63.515°W, and for 50 nodes along the VF transect, between 42.386°S and 42.986°S. These numbers of nodes provide a separation between nodes of about 1.4 km along each transect, coincident with the grid model, whose outputs are the inputs used in the present model. Using one year of daily outputs, the threshold gradient, the frontal percentage of occurrence, the sea surface temperature gradient and the frontal position were calculated.

The simulated SMF is detected from November to March, located ~8 km west of the position derived from satellite images (Fig. 3C, dashed line). The variability of the front position is lower than that estimated from satellite data. The lower variability is probably associated with the fact that the model simulates only a few processes and uses smooth forcing (climatological means). The surface temperature gradients are higher than those observed in the satellite images (Fig. 3B). The model succeeds in simulating the frontal displacement to shallower and deeper areas while the heat flux increases and decreases, respectively. A simple numerical experiment was carried out in order to explore the possible

relationship between heat flux and frontal displacement. Two simulations were performed changing the heat flux phase one month forward and one month backward, and keeping the remaining variables unchanged. The results showed that the easternmost (shallower) position of the front is reached following the maximum heat flux (not shown). These results suggest that seasonal fluctuations in the frontal position are mainly driven by the surface heat flux regardless of the observed changes in wind, since it has a very low seasonality and it has little relevance in controlling frontal position (Simpson et al., 1978).

The simulated VF is detected with a high percentage of occurrence between November and March (Fig. 4A). The simulated front is located south of the observed front and surface temperature gradients are 2-fold larger than observed. Fluctuations in frontal position are lower in magnitude than those observed in the satellite images. However, as shown by the analysis of satellite images, the simulated front displaces northwards (to shallower waters) and southwards (to deeper waters) as the heat flux increases and decreases, respectively (dotted line in Fig. 4C). The overestimated sea surface temperature gradients in both fronts might be due to an underestimation of wind driven mixing, which is likely to occur as a result of forcing the model with climatological winds which do not present synoptic scale variability. This situation would lead to warmer SSTs on the stratified side of the front and consequently to higher surface temperature gradients.

Simulations do not reproduce the frontal displacement during the spring–neap cycle on either of the fronts. However, the surface temperature gradients display fortnightly frequency variability particularly in the early Austral spring (October–November). During this period the surface mixed layer is shallow and the changes in the bottom layer thickness following spring–neap fluctuations generate significant changes in the mixed layer thickness. A shallower/deeper surface mixed layer transition could induce changes in the SST, leading to changes in temperature gradient across the front. These results suggest that fortnightly variability of tidal mixing simulated by the model succeeds in changing the relative thickness of the bottom and surface mixed layers, but is too weak to achieve complete vertical mixing. This same effect could explain both the observed changes in temperature gradient and the absence of front displacement at a fortnightly time scale.

The simulated fronts are both located on deeper and steeper regions than those observed from the satellite images (Figs. 3C and 4C). This is probably a consequence of an overestimation of tidal vertical mixing at a semidiurnal time scale relative to wind mixing. The stronger tidal mixing would simultaneously homogenize a deeper water column and, consequently, increase the surface temperature gradient (Figs. 3B and 4B). Although the predicted current velocities by the model are significantly higher during spring tide, the associated increased vertical mixing does not lead to an observable change in the front position, probably due to the steeper bottom slope. This limitation to simulate changes in front position following the spring–neap cycle is reflected in the lower dispersion of monthly mean position (much smaller SD in Figs. 3C and 4C) relative to those observed in satellite images.

On the other hand, using a model similar to that used in this work, Simpson and Sharples (1994) showed that the efficiency of mixing depends on the tidal currents' polarization. When the tidal current is highly polarized the mixing can be significantly greater or smaller according to the direction of polarization. The model implemented in this study was run with the polarization estimates from the model of Tonini (2010). Simpson and Sharples (1994) conclude that if the polarization modulus $|P|$ is <0.3 (as in our case) the influence of rotation will be small and control of frontal boundaries will primarily rest on the energy constraint. Thus, it does not appear that our model results are affected by incorrect polarization.

5. Summary and discussion

Frontal space and time variability are important because they delimit the region of enhanced primary production and can impact the associated fishing grounds. The frontal position is strongly associated with the bottom topography, and the energy required to displace a tidal front is higher as the bottom slope increases.

The SMF is characterized by relatively strong SST gradients during the stratified season. The front displaces to shallower waters (eastward) from October to January and remains almost invariant during the summer. In this period, the average displacement of the front is 1–2 km, similar in magnitude to the spatial resolution of satellite images (Fig. 3C). Similarly, the VF shows a northward displacement of the monthly averaged position from November until January–February (Fig. 4C). A simple, one-dimensional numerical model reproduces the frontal displacements toward shallow waters while the heat flux increases, suggesting that variations in wind intensity are not important in setting the observed seasonal displacements.

The relatively high SD observed around monthly average displacements indicates that there is relatively large variability at higher frequency. The frontal position anomalies relative to the monthly mean positions averaged for each day of the lunar cycle were used to analyze the influence of spring–neap cycle on the frontal position (Fig. 5A and B). A clear oscillation of around 10 km amplitude (SD$\sim$5 km) was observed in the SMF at a fortnightly frequency. In the same frequency, the VF displays oscillations of higher amplitude ($\sim$15 km), but the SDs are of similar magnitude ($\sim$15–20 km). These observations provide the first evidence of fortnightly oscillations in fronts in the ACS.

In turn, few references to tidal front fortnightly variability are found in the literature. Simpson and Bowers (1981) found variations in the position of tidal fronts of the order of 4 km during the spring–neap transition in the Irish Sea. Even after removing semidiurnal and fortnightly fluctuations, they observed frontal displacements of around 7 km. Paden et al. (1991) observed $\sim$10–15 km frontal displacements over the spring–neap tidal cycle in a tidal front in the Gulf of California. On the other hand, Kasai et al. (1999) found that the well defined thermohaline front that separates the stratified Clyde Sea water from the vertically well mixed off-shore water of the North Channel oscillates 3–5 km back and forth with the tidal currents. In contrast with the fronts in the ACS, in the Clyde Sea front the buoyancy is due to both surface heat exchange and freshwater run-off, and the density structure is governed by salinity. Hopkins and Polton (2012) observed fortnightly displacements of 5–35 km of a thermohaline front associated with changes in tidal mixing intensity in Liverpool Bay. They described a semidiurnal tidal oscillation of 5–10 km overlapping the fortnightly oscillation. The influence of spring–neap cycle on nutrient flows at the shelf edge of the Celtic Sea was analyzed by Sharples et al. (2007). They found that the spring tide nitrate flux was about 3 times higher than at neap tide, associated with a higher tidal dissipation. Rogachev et al. (2001) also found strong variations in salinity, dissolved oxygen and silicate concentrations associated with a fortnightly cycle in the sea of Okhotsk, and discussed a fortnightly biological resonance following cyclic variations in nutrient supply. Carreto et al. (1985) have observed a sharp transition of $>4\ \mu$M of nitrates across the summer thermocline on the stratified side of the VF, and relatively high concentrations throughout the water column on the homogeneous side of the front. Thus, tidal mixing across the ACS fronts can also play a significant role on the nutrient fluxes.

Based on the analysis of a high-resolution numerical simulation Tonini (2010) found a surface displacement of the VF of approximately 20 km, associated with spring–neap transitions. Also, idealized two-dimensional numerical simulations in a section

across VF produced cross-frontal variations of 10–15 km during a semidiurnal cycle (M_2) and a front displacement of approximately 35 km with increasing vertical stratification from September to December (Franco, 2013). However, it should be noted that in these two previous simulations the transect orientation differs from that used in this work. The model used in this study failed in detecting fortnightly position oscillations, but succeeded in detecting gradient intensity oscillations at this frequency.

Ou et al. (2003) postulated that vertically integrated diffusion is responsible for the frontal position, especially for winter haline fronts. This theory predicts that the frontal depth of the frontal area varies as the square root of the tidal amplitude. The Simpson–Hunter criterion (Simpson and Hunter, 1974), based on a balance of mechanical mixing (more applicable to tidal fronts), relates the bottom depth to the cube of the tidal current. This criterion overestimates the influence of the spring–neap cycle, unless a feedback factor that inhibits vertical mixing is considered (see Simpson and Sharples, 1994 and references herein). Ou et al. (2003) indicate that although their relationship could be weak, the dependence between water depth and tidal current velocity may lead to detectable frontal migration between spring and neap cycles, although the authors did not evaluate this process. In our study the neap and spring velocities are $\sim$0.6 m s^{-1} and 1 m s^{-1}, respectively (Tonini, 2010). This suggests that the depth at which the front is located should vary by a factor of 1.29, applying the relationship suggested by Ou et al. (2003). In both fronts the detection depth is about 70 m (Figs. 3 and 4), i.e. the depth should vary fortnightly by at least about 20 m. The average horizontal displacement of frontal position is around 10 and 20 km for SMF and VF, respectively (Fig. 5). Although the bathymetry (see Figs. 3 and 4) does not seem to have a marked slope as this theoretical prediction requires, the discrepancies between the observations and the theoretical predictions are not large. Additionally, the smoothing of frontal displacements facilitates the visualization of the fortnightly cycle but reduces the range of the position variability.

Although the dynamics of tidal fronts are governed by the effects of tidal currents, surface winds and heat fluxes, the frontal displacements are also strongly influenced by the peculiarities of the bottom topography, the tidal fortnightly variability, and frontal instabilities. To some extent the variability of the frontal position has been masked by the relatively large SD. Possible ways to better understand the frontal displacement will require collection of in-situ observations capable of resolving these mesoscale displacements from hourly to seasonal time scales, while more complex numerical models may help disentangle the processes that control the observed variability.

Acknowledgments

We thank Antonio Gagliardini for providing the AVHRR satellite data, G. Williams for providing information about the processing of the images, M. Tonini for supplying the ROMS model data, B. Franco for sharing the results of her numerical simulations prior to publication and F. Dellatorre for his thorough review. This work was completed with support from CONICET (Grant PIP 112 200801 03105), Argentina, and Grant CRN2076 from the Inter-American Institute for Global Change Research (US National Science Foundation Grant 0452325).

References

Acha, E.M., Mianzan, H.W., Guerrero, R.A., Favero, M., Bava, J., 2004. Marine fronts at the continental shelves of austral South America: physical and ecological processes. J. Mar. Syst. 44, 83–105.

Alemany, D., Acha, E.M., Iribarne, O., 2009. The relationship between marine fronts and fish biodiversity in the Patagonian Shelf Large Marine Ecosystem. J. Biogeogr. 36, 2111–2124.

Apel, J.R., 1980. Satellite sensing of ocean surface dynamics. Ann. Rev. Earth Planet. Sci. 8, 303–342.

Badin, G., Williams, R.G., Holt, J.T., Fernand, L.J., 2009. Are mesoscale eddies in shelf seas formed by baroclinic instability of tidal fronts? J. Geophys. Res. 114, C10021.

Balech, E., Ehrlich, M.D., 2008. Esquema Biogeográfico del Mar Argentino. Rev. Invest. Desarr. Pesq. N19, pp. 45–75.

Bava, J., D.A. Gagliardini, A.I. Dogliotti, C.A. Lasta, 2002. Annual distribution and variability of remotely sensed sea surface temperature fronts in the Southwestern Atlantic Ocean. In: Proceedings of the 29th International Symposium on Remote Sensing of Environment Buenos. Aires, Argentina.

Bianchi, A.A., Pino, D.R., Perlender, H.G. I., Osiroff, A.P., Segura, V., Lutz, V., Clara, M. L., Balestrini, C.F., Piola, A.R., 2009. Annual balance and seasonal variability of sea–air CO_2 fluxes in the Patagonia Sea: their relationship with fronts and chlorophyll distribution. J. Geophys. Res. 114, C03018.

Bogazzi, E., Baldoni, A., Rivas, A.L., Martos, P., Reta, R., Orensanz, J., Lasta, M., Dell'Arciprete, P., Werner, F., 2005. Spatial correspondence between areas of concentration of Patagonian scallop and frontal systems in the southwestern Atlantic. Fish. Oceanogr. 14 (5), 359–376.

Carreto, J.I., Negri, R.H., Benavides, H.R., Akselman, R., 1985. Toxic dinoflagellates blooms in the Argentine Sea. In: Anderson, D.M, White, A.W, Baden, D.G. (Eds.), Toxic Dinoflagellates, eds Eslevier, NY, pp. 147–152

Carreto, J.I., Benavides, H.R., Negri, R.H., Glorioso, P.D., 1986. Toxic red tide in the Argentine Sea: phytoplankton distribution and survival of the toxic dinoflagellate *Gonyaulax excavata* in frontal area. J. Plankton Res. 8, 15–28.

Davis, A.M., Sauvel, J., Evans, J., 1985. Computing near coastal tidal dynamics from observations and a numerical model. Cont. Shelf Res. V 4-3, 341–366.

Egbert, G.D., Ray, R.D., 2000. Significant dissipation of tidal energy in the deep ocean inferred from satellite altimeter data. Nature 405, 775–778.

Egbert, G.D., Ray, R.D., 2001. Estimates of M2 tidal dissipation from TOPEX/Poseidon altimeter data. J. Geophys. Res. 106, 22475–22502.

Egbert, G.D., Ray, R.D., Bills, B.G., 2004. Numerical modeling of the global semidiurnal tide in the present day and in the last glacial. J. Geophys. Res. 109, C03003, http://dx.doi.org/10.1029/2003JC001973.

Franco, B.C., 2013. Procesos acoplados bento-pelágicos relacionados con el establecimiento y deriva larval de la vieira patagónica (*Zygochlamys patagonica*) en el Océano Atlántico sudoeste, Doctoral Dissertation. Universidad de Buenos Aires. 232pp.

Gagliardini, D.A., Rivas, A.L., 2004. Environmental characteristics of San Matías gulf obtained from Landsat-TM and ETM+ data. Gayana 68 (2), 186–193.

Gagliardini, D.A., Aliotta, S., Dogliotti, A.I., Clemente-Colón, P., 2005. Identification of bed forms through ERS SAR images in San Matías Gulf, Argentina. J. Coast. Res. 21-1, 193–201.

Glorioso, P.D., Flather, R.A., 1995. A barotropic model of the currents SE South America. J. Geophys. Res. 100, 13427–13440.

Glorioso, P.D., Flather, R.A., 1997. The Patagonian Shelf tides. Prog. Oceanogr. 40, 263–283.

Glorioso, P.D., Simpson, J.H., 1994. Numerical modeling of the M_2 tide on the northern Patagonian Shelf. Cont. Shelf Res. 14, 267–278.

Hoffman, J.A.J, Núñez y, M.N., Piccolo, M.C, 1997. Características Climáticas del Atlántico Sudoccidental "El Mar Argentino y sus Recursos Pesqueros". In: Boschi, por E (Ed.), Inst. Nac. De Investigación y Desarrollo Pesquero. Mar del Plata, Argentina, pp. 163–193 (editado)

Hopkins, J., Polton, J.A., 2012. Scales and structure of frontal adjustment and freshwater export in a region of freshwater influence. Ocean Dyn. 62, 45–62.

Kalnay, E, et al., 1996. The NCEP/NCAR 40-year Reanalysis Project. Bull. Am. Meteorol. Soc. 77 (3), 437–471.

Kasai, A., Rippeth, T.P., Simpson, J.H., 1999. Density and flow structure in the Clyde Sea front. Cont. Shelf Res. 19, 1833–1848.

Kelly, K.A., 1985. Separating clouds from ocean in infrared images. Remote Sens. Environ. 17, 67–83.

Le Boyer, A., Cambon, G, Daniault, N., Herbette, S., Le Cann, B., Marie, L., Morin, P., 2009. Observations of the Ushant tidal front in September 2007. Cont. Shelf Res. 29, 1026–1037.

Loder, J.W., Platt, T., 1985. Physical controls on phytoplankton production at tidal fronts. In: Gibbs, P.E. (Ed.), Proceedings of the 19th European Marine Biology Symposium. Cambridge University Press, pp. 3–21

Monaldo, F., 1996. Primer on the Estimation of Sea Surface Temperature Using TeraScan Processing of NOAA AVHRR Satellite Data, Version 2.0, S1R-96M-03, Johns Hopkins University Applied Physics Laboratory.

Ocampo-Reinaldo, M., González, R., Williams, G., Storero, L.P., Romero, M.A., Narvarte, M., Gagliardini, D.A., 2013. Spatial patterns of the Argentine hake *Merluccius hubbsi* and oceanographic processes in a semi-enclosed Patagonian ecosystem. Mar. Biol. Res. 9 (4), 394–406.

Ou, H.W., Dong, C., Chen, D., 2003. Tidal diffusivity: a mechanism for frontogenesis. J. Phys. Oceanogr. 33, 840–847.

Paden, C.A., Abbott, M.R., Winant, C.D., 1991. Tidal and atmospheric forcing of the upper ocean in the Gulf of California: 1. Sea surface temperature variability. J. Geophys. Res. 96 (C10), 18337–18359.

Palma, E.D., Matano, R.P., Piola, A.R., 2004. Three dimensional barotropic response of the southwestern Atlantic shelf circulation to tidal and wind forcing. J. Geophys. Res. 109, http://dx.doi.org/10.1029/ 2004JC002315 (C08014).

Pierce, J.W., Sieguel, F.R., Urien, C.M., 1969. Topografía submarina del Golfo San Matías. In: Proceedings of the VI Jornadas Geológicas Argentinas (Buenos Aires, Argentina). Actas III, pp.127–140.
Pingree, R.D., 1978. Cyclonic eddies and cross-frontal mixing. J. Mar. Biol. Assoc. UK 58, 955–963.
Pingree, R.D., 1979. Baroclinic eddies bordering the celtic sea in late summer. J. Mar. Biol. Assoc. UK 59, 689–698.
Podestá, G.P., Browder, J.A., Hoey, J.J., 1993. Exploring the association between swordfish catch rates and thermal fronts on U.S. longline grounds in the western North Atlantic. Con. Shelf Res. 13 (2-3), 253–277.
Polzin, K.L., Toole, J.M., Ledwell, J.R., Schmitt, R.W., 1997. Spatial variability of turbulent mixing in the abyssal ocean. Science 276, 93, http://dx.doi.org/10.1126/science.276.5309.93.
Rivas, A.L., 1990. Heat balance and annual variation of mean temperature in the North-Patagonian gulfs. Oceanol. Acta 13, 265–272.
Rivas, A.L., 1994. Spatial variation of the annual cycle of temperature in the patagonian shelf between 40 and 50° of the south latitude. Cont. Shelf Res. 14, 1539–1554.
Rivas, A.L., Dogliotti, A.I., Gagliardini, D.A., 2006. Satellite-measured surface chlorophyll variability in the Patagonian shelf. Cont. Shelf Res. 26, 703–720.
Rivas, A.L., 2006. Quantitative estimation of the influence of surface thermal fronts over chlorophyll concentration at the Patagonian shelf. J. Mar. Syst. 63, 183–190.
Rivas, A.L., Pisoni, J.P., 2010. Identification, characteristics and seasonal evolution of surface thermal fronts in the Argentinean Continental Shelf. J. Mar. Syst. 79, 134–143.
Rogachev, K.A., Carmack, E.C., Salomatin, A.S., Alexanina, M.G., 2001. Lunar fortnightly modulation of tidal mixing near Kashevarov Bank, Sea of Okhotsk, and its impacts on biota and sea ice. Prog. Oceanogr. 49, 373–390.
Romero, S.I., Piola, A.R., Charo, M., Garcia, C.A.E., 2006. Chlorophyll-a variability off Patagonia based on SeaWiFS data. J. Geophys. Res. 111 (C5), C05021.
Sabatini, M., Martos, P., 2002. Mesozooplankton features in a frontal area off northern Patagonia (Argentina) during spring 1995 and 1998. Sci. Mar. 66 (3), 215–232.
Sharples, J., 1999. Investigating the seasonal vertical structure of phytoplankton in shelf seas. Mar. Models 1 (1–4), 3–38.
Sharples, J., Tett, P., 1994. Modelling the effect of physical variability on the midwater chlorophyll maximum. J. Mar. Res. 52 (2), 219–238.
Sharples, J., Tweddle, J.F., Green, J.A.M., Palmer, M.R., Kim, Y-N., Hickman, A.E., Holligan, P.M., Moore, C.M., Rippeth, T.P., Simpson, J.H., Krivtsov, V., 2007. Spring-neap modulation of internal tide mixing and vertical nitrate fluxes at a shelf edge in summer. Limnol. Oceanogr. 52 (5), 1735–1747.
Simpson, J.H., Hunter, J.R., 1974. Fronts in the Irish Sea. Nature 250, 404–406.
Simpson, J.H., Allen, C.M., Morris, N.C.G., 1978. Fronts in the Continental Shelf. J. Geophys. Res. 83 (C9), 4607–4614.
Simpson, J.H., Bowers, D., 1981. Models of stratification and frontal movement in shelf seas. Deep-Sea Res. 28, 727–738.
Simpson, J.H., Sharples, J., 1994. Does the Earth's rotation influence the location of the shelf sea fronts? J. Geophys. Res. 99, 3315–3319.
Simpson, J.H., Crawford, W.R., Rippeth, T.P., Campbell, A.R., Cheok, J.V.S., 1996. The vertical structure of turbulent dissipation in shelf seas. J. Phys. Oceanogr. 26, 1579–1590.
Tonini, M.H, 2010. Modelado Numérico del Ecosistema del los Gofos Norpatagónicos. Doctoral Dissertation. Universidad Nacional del Sur. Bahía Blanca. 255pp.
Tonini, M.H., Palma, E.D., Piola, A.R., 2013. A numerical study of gyres, thermal fronts and seasonal circulation in austral semi-enclosed gulfs. Cont. Shelf Res. 65, 97–110.
Williams, G.N., Sapoznik, M., Ocampo-Reinaldo, M., Solís, M., Narvarte, M., González, R., Esteves, J.L., Gagliardini, D.A., 2010. Comparison of AVHRR and SeaWiFS imagery with fishing activity and in-situ data in San Matías Gulf, Argentina. Int. J. Remote Sensing 31 (17), 4531–4542.